Colloquium: Manipulating quantum entanglement with atoms and photons in a cavity

J. M. Raimond, M. Brune, and S. Haroche

Laboratoire Kastler Brossel,* Département de Physique de l'Ecole normale supérieure, 24 rue Lhomond, F-75231, France

After they have interacted, quantum particles generally behave as a single nonseparable entangled system. The concept of entanglement plays an essential role in quantum physics. We have performed entanglement experiments with Rydberg atoms and microwave photons in a cavity and tested quantum mechanics in situations of increasing complexity. Entanglement resulted either from a resonant exchange of energy between atoms and the cavity field or from dispersive energy shifts affecting atoms and photons when they were not resonant. With two entangled particles (two atoms or one atom and a photon), we have realized new versions of the Einstein-Podolsky-Rosen situation. The detection of one particle projected the other, at a distance, in a correlated state. This process could be viewed as an elementary measurement, one particle being a "meter" measuring the other. We have performed a "quantum nondemolition" measurement of a single photon, which we detected repeatedly without destroying it. Entanglement is also essential to understand decoherence, the process accounting for the classical appearance of the macroscopic world. A mesoscopic superposition of states ("Schrödinger cat") gets rapidly entangled with its environment, losing its quantum coherence. We have prepared a Schrödinger cat made of a few photons and studied the dynamics of its decoherence, in an experiment which constitutes a glimpse at the quantum/classical boundary. We have also investigated entanglement as a resource for the processing of quantum information. By using quantum two-state systems (qubits) instead of classical bits of information, one can perform logical operations exploiting quantum interferences and taking advantage of the properties of entanglement. Manipulating as qubits atoms and photons in a cavity, we have operated a quantum gate and applied it to the generation of a complex three-particle entangled state. We finally discuss the perspectives opened by these experiments for further fundamental studies.

CONTENTS

I. INTRODUCTION

The superposition principle is at the heart of the most intriguing features of the microscopic world. A quantum system may exist in a linear superposition of different eigenstates of an observable. It is then, in some way, "suspended" between different classical realities: a particle can be at two positions at the same time, a spin may point simultaneously towards two different directions, etc. When a measurement is performed, only one of these possibilities is actualized and the system is projected onto the corresponding eigenstate (wave-function collapse). It is impossible to get a classical intuitive representation of these superpositions. Their oddity becomes evident when one tries to transpose them to the macroscopic scale, as in the famous "Schrödinger cat" metaphor (Schrödinger, 1935), describing a cat suspended between life and death.

When the superposition principle is applied to composite systems, it leads to the essential concept of entanglement. After two classical systems have interacted, each must be in a well-defined individual state, corresponding to definite results for any experiment. After two quantum particles have interacted, however, they can no longer be described independently of each other. Their "entangled" state is not a tensor product of eigenstates of observables pertaining to the two particles, which would describe independent systems with well-defined properties. It is instead a superposition of such products. The state of one particle is determined by a measurement performed on the other. Moreover, the same entangled state can be written in different forms, corresponding to different sets of noncommuting ob-

servables for the two particles. The state of one particle thus also depends upon the *nature* of the observable one has decided to measure on the other particle, even if the choice is made after the particles have separated. These quantum correlations are independent of the particles spatial separation and introduce a fundamental nonlocal aspect in the quantum world.

The nonclassical properties of entangled states are clearly illustrated by the Einstein, Podolsky, and Rosen (EPR) (1935) situation. Following Bohm's (1951) analysis of the EPR problem, let us consider two spin-1/2 systems in the combined state:

$$|\Psi_{EPR}\rangle = \frac{1}{\sqrt{2}}(|+_1, -_2\rangle - |-_1, +_2\rangle) \qquad (1.1)$$

$$= \frac{1}{\sqrt{2}}(|+_{\mathbf{u},1}, -_{\mathbf{u},2}\rangle - |-_{\mathbf{u},1}, +_{\mathbf{u},2}\rangle), \qquad (1.2)$$

where $|\pm\rangle$ are the eigenstates of the spins along the Oz axis ($|\pm_{\mathbf{u}}\rangle$ the states along an arbitrary direction $\mathbf{u}$), and the indices distinguish the two spins. $|\Psi_{EPR}\rangle$ being the rotation-invariant spin-singlet state, it takes the same form, as shown above, for any orientation of the quantization axis. All features of entangled states are clearly apparent in these expressions. Before any measurement, neither 1 nor 2 are described by a well-defined state. After 1 has been measured along axis $\mathbf{u}$, 2 points in the opposite direction along the same axis.

These basis-independent correlations cannot be understood in classical terms. Moreover, the statistical predictions of quantum mechanics contradict the results of any "local" theory, as they are expressed by the famous Bell inequalities (Bell, 1964; Aspect, Dalibard, and Roger, 1982). The experimental violation of these inequalities (for reviews, see Zeilinger, 1998; Aspect, 1999) has vindicated quantum theory. More complex entangled states lead also to striking violations of locality. Greenberger, Horne, and Zeilinger (GHZ) (1990) proposed to use triplets of spin particles in the entangled state:

$$|\Psi_{GHZ}\rangle = \frac{1}{\sqrt{2}}(|+_1, +_2, +_3\rangle + |-_1, -_2, -_3\rangle). \qquad (1.3)$$

A single ideal experiment provides, in this state, opposite results for quantum mechanics and local theories.

Entanglement is also at the heart of quantum measurement. When two systems are in an entangled state, each of them can reveal information about the other, behaving as a measuring device. In a realistic measurement of a microscopic system, however, the meter is macroscopic. The situation is again reminiscent of the Schrödinger cat metaphor, with a meter evolving into a superposition of states with different classical properties. Such superpositions are extremely sensitive to the dissipative coupling between the meter and its environment. Entangled states involving macroscopic meters are rapidly transformed into statistical mixtures of product states, each of which describes the meter in a well-

defined configuration correlated to the microscopic system in a corresponding eigenstate. This fast relaxation process is called "decoherence" (Zurek, 1981, 1982, 1991; Caldeira and Leggett, 1983; Omnès, 1994). In fact, decoherence itself involves entanglement. The meter gets entangled with its environment. As the information leaks into the environment, the meter's state is obtained by tracing over the environment variables, leading to the final statistical mixture. This analysis is fully consistent with the Copenhagen description of a measurement.

Beyond these fundamental aspects, entangled states might have important applications for information transmission or processing. Elements of binary information can be coded in two-state quantum systems called qubits (DiVincenzo, 1995; Ekert and Josza, 1996). Contrary to ordinary bits, qubits can be in a quantum superposition of different logical values and combined into entangled states. EPR correlations between two qubits can be used to perform cryptographic key distribution (Ekert, 1991). By sharing EPR pairs, two operators can communicate in absolute secrecy. Quantum state teleportation (Bennett *et al.*, 1993) also uses the nonlocal features of the EPR pair to transmit the quantum state of a particle from one place to another at light velocity.[1]

More sophisticated entanglement manipulations could be used to perform interesting tasks, such as entanglement purification [i.e., the extraction of a subset of pure EPR states from a larger ensemble of particle pairs in a statistical mixture (van Enk, Cirac, and Zoller, 1997)]. Quantum error correction codes (Steane, 1996) can be used to improve the quality of quantum transmissions (Ekert and Macchiavelo, 1996). Very complex entangled states could even be used to perform calculations out of the reach of ordinary computers. Factorization of integers (Shor, 1994; Ekert and Josza, 1996), random searches (Grover, 1997), quantum systems simulations (Lloyd, 1996) could be performed by a "quantum computer" manipulating large sets of entangled qubits and operating exponentially faster than a classical computer. The qubits entanglement would be realized by small "entangling machines," called "quantum gates" (DiVincenzo, 1995; Ekert and Josza, 1996). They couple two qubits through a well-controlled conditional dynamics operation. The evolution of the state of one qubit (the "target") depends upon the state of the other (the "control"), which usually remains unaltered. A deterministic combination of gate operations leads to the final state, in which the "result" can be measured. These macroscopic

----

[1]Note that in all these schemes, as well as in the original EPR situation, no information can be transmitted faster than light even though the quantum collapse can be viewed as instantaneous. In the Bell's inequalities experiments, for example, each operator measures a random sequence on which the other has no deterministic control. All the information is contained in the correlations between the sequences measured by the observers. Classical information exchange is required to check these correlations. In teleportation, no state is received before a classical signal has been transmitted. There is never contradiction between nonlocality and relativistic causality.

qubits systems are, however, utterly sensitive to decoherence (Haroche and Raimond, 1996), which appears thus as a very severe bottleneck for quantum computing.

Fundamental tests as well as potential applications have triggered a considerable interest for experiments on basic quantum mechanics. The manipulation of complex entangled states puts very severe constraints on the experimental techniques. The individual systems should be prepared in a well-defined initial quantum state. They should be very well isolated from the environment and interact strongly with each other, as required for the realization of quantum gates. Their state should be accurately detected, with a high efficiency. Furthermore, individual qubit addressing is required for the engineering of the most general entangled state, scalable to arbitrary numbers of qubits, as well as for performing fundamental tests of quantum measurement theory. Many propositions have been made to implement these requirements. Solid-state devices [mesoscopic conductors (Bouchiat *et al.*, 1999; Bertoni *et al.*, 2000), squids (Friedmann *et al.*, 2000; van der Wal *et al.*, 2000), single impurity spins, etc.] are under active consideration. Up to now, however, entanglement remains to be demonstrated in these systems. Nuclear magnetic resonance in liquid samples provides long relaxation times, spin-spin exchange interactions needed for quantum gates and sophisticated techniques developed for chemical analysis (Gershenfeld and Chuang, 1997; Jones, Mosca, and Hansen, 1998). Complex manipulations have been realized. However, they rely on very small deviations from thermal equilibrium and no clear-cut entanglement is involved (Braunstein, 1999; Schack and Caves, 1999). Moreover, measurements on individual spins are not feasible and only quantum averages can be detected.

Entanglement has been so far observed only in quantum optics. Photons in entangled states are spontaneously produced in atomic cascades or parametric down-conversion processes converting an incoming UV photon into two entangled visible ones. Polarization states can be easily manipulated, the photons propagating over long distances and being finally detected with a high efficiency. Entanglement between photons with different energies and times of arrival can also be realized (Tittel *et al.*, 2000). Recently, these experiments have greatly benefited from the progress in optical fiber communication technology. Tests of Bell inequalities (Aspect, Dalibard, and Roger, 1982; Zeilinger, 1998), creation of GHZ triplets and nonlocality tests (Pan *et al.*, 2000), teleportation of quantum states (Bouwmeester *et al.*, 1998; Boschi *et al.*, 1998; Furusawa *et al.*, 1998) have been performed. Sophisticated quantum cryptographic systems, on the verge of industrial development, use correlated photons (Rarity, Owens, and Tapster, 1994; Jennewein *et al.*, 2000; Naik *et al.*, 2000; Tittel *et al.*, 2000). In these experiments, entanglement results from the basic conservation laws in the initial spontaneous process and cannot be easily manipulated afterwards, due to the lack of an efficient photon-photon quantum gate.

Entanglement of slow or trapped matter particles offers other perspectives. Remarkable achievements have been obtained with trapped ions. Laser cooling techniques prepare a few ions in the vibrational ground state inside the trap. The long-lived internal structures can be entangled with the collective motion, providing quantum gate operation. Finally, laser induced fluorescence techniques provide a selective detection of the ionic state with an efficiency close to unity. Quantum gate operation (Monroe *et al.*, 1995) and both two-ion (Turchette *et al.*, 1998) and four-ion (Sackett *et al.*, 2000) entangled states have been demonstrated. Up to now, the condition of strong ion-ion coupling requires a very small spatial separation between the ions, making it difficult to address them individually.

Cavity quantum electrodynamics (CQED) (Berman, 1994) studies mixed atom/photon systems and offers other interesting tools for entanglement. A single two-level atom crossing a cavity mode gets entangled with the field, provided the coherent coupling overwhelms the dissipative processes ("strong-coupling regime"). Ordinary optical atomic transitions and very high finesse cavities make it possible to meet the strong-coupling conditions (Thompson *et al.*, 1992) and to observe interesting quantum effects (Münstermann *et al.*, 1999; Hood *et al.*, 2000). The very fast time evolution of these optical systems has not made it possible so far to investigate entanglement directly.

Microwave CQED, with Rydberg atoms crossing superconducting cavities one by one (Haroche and Raimond, 1994; Raithel *et al.*, 1994), offers an almost ideal system for entanglement studies. Relaxation rates are small and well understood. The atoms and the cavity can be prepared in pure states and the strong-coupling conditions are readily fulfilled. The atoms can be detected in a selective and sensitive way by field ionization. The time constants involved (millisecond range) are long enough to realize controlled and complex sequences. Finally, the quantum systems are separated by centimeter-scale distances and can be individually addressed.

This paper reviews Rydberg atom microwave CQED experiments on entanglement performed at ENS in Paris. In the spirit of a colloquium, we will focus on the main physical ideas, without insisting on experimental details, which can be found in review articles (Haroche, 1992; Maître *et al.*, 1997; Raimond and Haroche, 1999) or on our Web site (Raimond, 2000). Section II presents a rapid overview of the experimental techniques. Section III describes the resonant atom-field interaction. The quantum Rabi oscillation of the atom in the cavity (Brune *et al.*, 1996) provides all the ingredients to manipulate atom-cavity and atom-atom entanglement. These features are illustrated by the generation of an EPR atomic pair (Hagley *et al.*, 1997) in Sec. IV. We describe in Sec. V the realization of a quantum gate (Rauschenbeutel *et al.*, 1999). The next two sections describe applications of this gate. In Sec. VI, we analyze a nondestructive measurement of a single photon (Nogues *et al.*, 1999). In Sec. VII, we apply the quantum gate to the generation of an entangled triplet of the GHZ type
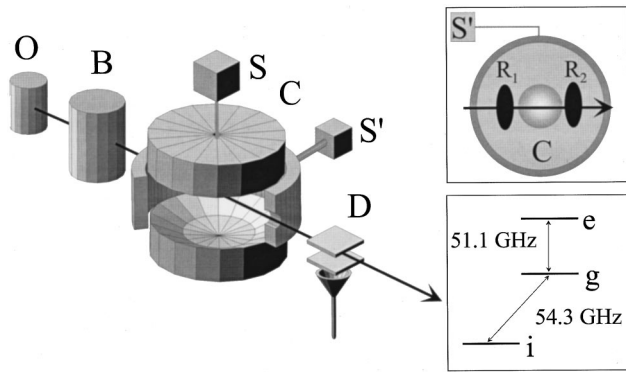
FIG. 1. Experimental apparatus. Top inset: top view of the cavity mode and of the two Ramsey field zones. Bottom inset: relevant circular levels.

(Rauschenbeutel *et al.*, 2000). Finally, Sec. VIII reviews atom-cavity entanglement obtained through nonresonant dispersive interaction. We describe the generation of mesoscopic Schrödinger cat states of the field (Brune *et al.*, 1996) and the study of their decoherence dynamics. We conclude (Sec. IX) by presenting some perspectives opened by these experiments.

II. THE CAVITY QED ENTANGLING MACHINE

The experimental setup is sketched in Fig. 1.[2] Circular Rydberg atoms are produced in zone B by the excitation of a velocity-selected rubidium atomic beam effusing from oven O. They cross one by one a high quality superconducting cavity C and are finally detected by the field ionization detector D. The whole setup is cooled to around 1 K to minimize thermal field noise.

A. The circular Rydberg atoms

Circular Rydberg states (Hulet and Kleppner, 1983) correspond to large principal and maximum orbital and magnetic quantum numbers. The valence electron orbital is a thin torus centered on the atom's core, revealing quantum position fluctuations around the classical Bohr orbit. According to the correspondence principle, the properties of these states can be understood in classical terms. The transitions between neighboring circular states fall in the millimeter-wave domain for principal quantum numbers of the order of 50. Our experiments involve the three circular levels with principal quantum numbers 51, 50, and 49, called e, g, and i, respectively (see bottom inset in Fig. 1). The $e{\Leftrightarrow}g$ and $g{\Leftrightarrow}i$ transitions are at 51.1 and 54.3 GHz, respectively. The degeneracy of the Rydberg manifold is lifted by a small electric field isolating the e, g, and i states from the other noncircular levels. This field stabilizes the highly aniso-

tropic orbit (Gross and Liang, 1986) and can also be used to tune the $e{\Leftrightarrow}g$ and $g{\Leftrightarrow}i$ transition frequencies using the quadratic Stark effect. The dipole matrix elements of these transitions, proportional to the radius of the circular orbit, are very large (1250 atomic units for the $e{\Leftrightarrow}g$ transition).

The radiative lifetimes of e, g, and i—of the order of $T_{at}=30$ ms—are much longer than those for noncircular Rydberg states. In free space, the atoms would propagate a few meters at thermal velocity before decaying. Radiative decay is thus negligible along the 20-cm path inside the apparatus. The circular levels are ionized in a moderate electric field (128 V/cm for e) inside the detector D. The resulting electrons are accelerated and counted with a 40 (10)% detection efficiency. Since e, g, and i ionize in different fields, D is state selective. All our information about the system's state is provided by this field-ionization detection.

The preparation of the circular levels in B (Nussenzveig *et al.*, 1993) combines diode laser excitation and radiofrequency transitions. The process is pulsed and the atomic preparation time is known within a 2-μs interval. The circular state purity is $\geqslant 98\%$. Atomic velocity selection is an essential ingredient for the control of experimental sequences on each atom. It is performed by Doppler-selective optical pumping techniques (Hagley *et al.*, 1997; Nogues *et al.*, 1999) and results in a ± 2-m/s velocity class width. The position of each atom inside the apparatus is thus known with a ± 1-mm precision, an essential condition for individual atomic control.

The circular states excitation process prepares, on the average, 0.2 atoms per pulse, with Poisson statistics. Most pulses do not produce any atom and are rejected by the data acquisition software. In the remaining events, the probability for having two atoms in the same sample is about 20%. Half of these two-atom events are detected as such and rejected. Single atom events are thus selected with a 90% probability.

B. The superconducting cavity

The cavity is an open Fabry-Perot resonator, made of two carefully polished spherical niobium mirrors facing each other (with each mirror having a diameter of 50 mm and a radius of curvature of 40 mm and with a distance between mirrors equal to 27 mm). The cavity sustains a Gaussian TEM_{900} mode at frequency ω, with a $w=6$ mm waist, resonant or nearly resonant with the $e{\Leftrightarrow}g$ transition. This Fabry-Perot geometry is compatible with the application of a static electric field along the cavity axis, which is essential for the manipulation of circular states. Two small holes pierced in the center of the mirrors allow us to couple microwaves in and out of the cavity. The resonance frequency, tuned by mechanical translation of the mirrors, and the quality factor Q can thus be easily determined by cavity transmission experiments. A classical source S can be used to inject in C a small coherent field (Glauber, 1963).

Our best cavity so far has a photon storage time $T_r = 1$ ms (corresponding to $Q=3\times10^8$). This time is much

longer than the atom-cavity interaction time (a few tens of μs) allowing for atom-cavity entanglement to be produced before relaxation processes set in. To obtain this T_r value, we use an aluminum ring enclosing the open space between the mirrors (shown open in Fig. 1). It reflects the photons scattered by the mirror imperfections back into the mode and increases T_r by an order of magnitude. Small access and exit holes (3 mm diameter) are used for atomic beam access. Inhomogeneous stray electric fields in these holes shift randomly the atomic transition frequencies. Atomic coherences are spoiled, while the level populations are not affected. All entangled state manipulations must thus be realized inside the cavity-ring structure.

At thermal equilibrium, the cavity mode contains about 0.7 thermal photons on the average, originating from thermal field leaks. This field is removed at the beginning of each experimental sequence. We send across C a few atomic pulses, each containing a few atoms prepared in the lower level g of the transition resonant with C. These atoms efficiently absorb the thermal photons and reduce the effective field temperature (Nogues *et al.*, 1999). At the end of this "cooling sequence," the mean photon number is reduced down to 0.1. The experimental sequence then lasts a time no longer than $0.3T_r$ to limit thermal field buildup.

C. The atomic Ramsey interferometer

The atoms can be prepared in a superposition of energy states before the interaction with C and mixed again after this interaction, making it possible to prepare and analyze complex entangled states. For this purpose, we use two pulses of classical microwave radiation, applied in the zones called R_1 and R_2 in the top inset of Fig. 1. These pulses are generated by a second microwave source S' and injected in the cavity structure through a small hole in the ring. This auxiliary microwave field produces a standing-wave pattern inside the ring-mirror structure. Antinodes of this pattern, sandwiching the central cavity mode, are used to perform the pulses at the time an atom is crossing them. Different sequences of pulses can be applied on successive atoms by commuting the field source S'. Note that the fields applied in R_1 and R_2 have a very short relaxation time (in the nanosecond range), much smaller than the decay time T_r in the cavity mode C. This explains why these pulses can be described classically and do not produce any entanglement between atom and radiation (Kim *et al.*, 1999). They can be considered as classical tools to manipulate the atomic state superpositions.

Applying to an atom two successive $\pi/2$ pulses, R_1 and R_2, at a frequency ω_r that is nearly resonant with an atomic transition, for instance, the $g \Leftrightarrow i$ transition at frequency ω_{gi}, one has a Ramsey separated field interferometer (Ramsey, 1985) (see Fig. 2). The pulses mixing Rydberg states act as atomic internal state "beam splitters." To be specific, the $\pi/2$ R_1 pulse can perform the transformations $|g\rangle \rightarrow (|g\rangle + |i\rangle)/\sqrt{2}$ and $|i\rangle \rightarrow (-|g\rangle + |i\rangle)/\sqrt{2}$. After a time delay T, the second microwave
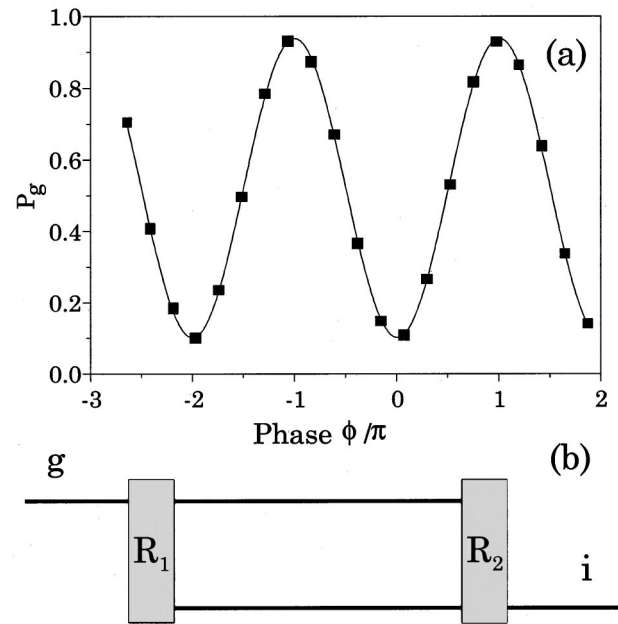

FIG. 2. Ramsey fringes. (a) Signal observed for the $g \Leftrightarrow i$ transition. Probability P_g for detecting the atom in g versus the phase difference ϕ between the two $\pi/2$ pulses R_1 and R_2 expressed in units of π. The points are experimental, the line is a sine fit. (b) Diagram depicting the two paths followed by the atom in the Ramsey interferometer.

pulse produces the transformations $|g\rangle \rightarrow [|g\rangle + \exp(i\phi)|i\rangle]/\sqrt{2}$ and $|i\rangle \rightarrow [-\exp(-i\phi)|g\rangle + |i\rangle]/\sqrt{2}$ with $\phi = (\omega_r - \omega_{gi})T$ describing the phase difference accumulated between the microwave source S' and the atomic coherence during time T.

Given that an atom is prepared in level g before R_1, the probability P_i for detecting it in level i after R_2 is the squared sum of two amplitudes corresponding to two atomic paths inside the interferometer [sketched in Fig. 2(b)]. The relative phase of these two amplitudes is ϕ. By repeating the experiment many times, we reconstruct the $g \rightarrow i$ transition probability, which oscillates versus ϕ, exhibiting the well-known pattern of Ramsey fringes. Ideally, $P_g = 1 - P_i = (1 - \cos\phi)/2$. Experimentally, our fringes have an 85% contrast [Fig. 2(a)]. The interaction of the atoms with the quantum field in C, between R_1 and R_2, modifies the phase and the amplitude of the fringes, revealing useful information about the atom-field coupling.

In some experiments, R_1 and R_2 can be used separately to prepare or analyze an atomic state superposition. It is useful to describe the atom undergoing the $g \rightarrow i$ (or $g \rightarrow e$) transition as a pseudospin 1/2 represented by a vector whose tip lies on a "Bloch sphere" of unit radius. The energy eigenstates correspond to the spin pointing in the "vertical Oz" direction. The classical microwave field produces a rotation of this pseudospin on the Bloch sphere. A $\pi/2$ pulse, for instance, acting on an energy eigenstate results in a spin lying in the "horizontal xOy" plane. Zone R_1 can thus be used to inject in C a spin pointing in a selected direction. Zone R_2, which rotates the spin before its detection along the Oz direc-

tion in D, allows us to detect the spin along an arbitrary direction on the Bloch sphere. In the language of quantum information, the two-level systems are qubits, coding superpositions of $|0\rangle$ and $|1\rangle$ states. In this context, R_1 and R_2 allow us to perform the most general single qubits operations. For instance, the $\pi/2$ pulses are known as Hadamard transforms (Ekert and Josza, 1996).

III. THE QUANTUM RABI OSCILLATION

A. Vacuum Rabi oscillation

The entangling mechanism in our experiments is based on the atom-cavity-field interaction. The simplest situation corresponds to an atom in level e entering the cavity, initially in its vacuum state $|0\rangle$. The cavity mode frequency ω is equal to the $e \Leftrightarrow g$ transition frequency ω_{eg}. The initial atom-cavity state $|e,0\rangle$ is coupled by dipole emission to $|g,1\rangle$, describing an atom in the lower state g and a cavity containing one photon. Quantum oscillations are expected between these two states (Haroche, 1992). These "vacuum Rabi oscillations" (Rempe, Walther, and Klein, 1987; Brune *et al.*, 1996) correspond to the oscillatory regime of spontaneous emission in a high Q cavity.

Quantitatively, the situation is described by the well-known Jaynes and Cummings (1963) Hamiltonian:

$$H = \hbar \omega_{eg} \sigma_z + \hbar \omega (a^\dagger a + 1/2) - i \frac{\hbar \Omega}{2} f(x)(\sigma_+ a - \sigma_- a^\dagger),$$
(3.1)

where a and $a^\dagger$ are the photon annihilation and creation operators in the cavity mode, and σ_z, σ_+, and σ_- are the Pauli matrices of the atomic pseudospin. The atom-field coupling constant $\Omega/2$ is equal to $d\mathcal{E}_0/\hbar$, where $\mathcal{E}_0 = 1.5\,\text{mV/m}$ is the rms vacuum field at the cavity center and d is the dipole matrix element for the $e \Leftrightarrow g$ transition ($\Omega/2\pi = 47\,\text{kHz}$). The cavity mode Gaussian structure is described by the real function $f(x) = \exp(-x^2/w^2)$ ($x \propto vt$ is the atomic position along the beam, with $x=0$ on the cavity axis).

Let us consider first an atom at cavity center $x=0$ with $v=0$. If the system starts at time $t=0$ from $|e,0\rangle$ its state at time t is

$$|\Psi_e(t)\rangle = \cos(\Omega t/2)|e,0\rangle + \sin(\Omega t/2)|g,1\rangle.$$
(3.2)

If the system starts in state $|g,1\rangle$ instead, its state becomes at time t:

$$|\Psi_g(t)\rangle = \cos(\Omega t/2)|g,1\rangle - \sin(\Omega t/2)|e,0\rangle$$
(3.3)

(we use here the interaction representation). In general, these expressions describe a time-varying entanglement between the atomic and cavity systems. When the atom moves across the cavity, these expressions apply provided we replace t by an effective interaction time t_i taking into account the spatial variation of the coupling. When the atom interacts resonantly with the cavity across the full mode structure, $t_i = \sqrt{\pi} w/v$. Note that the
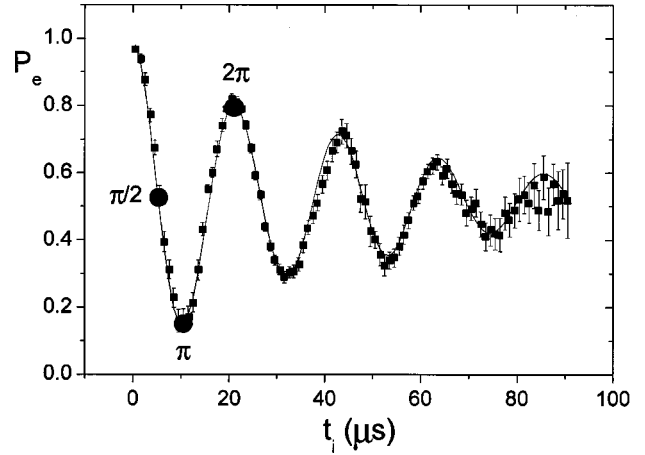

FIG. 3. Vacuum Rabi oscillations. The atom in state e enters an empty resonant cavity. P_e denotes the probability for detecting the atom in e as a function of the effective interaction time t_i. Three important interaction times (corresponding to the $\pi/2$, π, and 2π Rabi rotations) are indicated.

atom-field entanglement is "frozen" when the atom leaves the cavity mode. The entanglement becomes then nonlocal.

We have observed (Fig. 3) the quantum Rabi oscillation in vacuum by measuring the probability $P_e(t_i)$ that the atom remains in level e at time t_i (Brune *et al.*, 1996). Ideally, this probability oscillates at frequency $\Omega/2\pi$ (vacuum Rabi frequency):

$$P_e = \frac{1 + \cos \Omega t_i}{2}.$$
(3.4)

The time t_i is determined by the atomic velocity. The damping of the experimental signal is mainly due to technical imperfections. During the first Rabi oscillation, a wide variety of atom-cavity entangled states can be obtained with high fidelity by choosing properly t_i.

B. Useful Rabi pulses

When $\Omega t_i = \pi/2$ ("$\pi/2$ Rabi rotation"), the final atom field state reads

$$|\Psi_{\pi/2}\rangle = \frac{1}{\sqrt{2}}(|e,0\rangle + |g,1\rangle).$$
(3.5)

With an appropriate pseudospin states definition, it is the EPR state of Eq. (1.1). The entanglement, created in a time of the order of 5 μs, lasts as long as the photon in the cavity (1 ms).

When $\Omega t_i = \pi$, the atom-cavity system, initially in $|e,0\rangle$, ends up in the nonentangled state $|g,1\rangle$. If the system starts from $|g,1\rangle$ instead, it ends up in $-|e,0\rangle$. This "π Rabi rotation" swaps the atom and cavity excitations. More generally, if the atom is initially in a superposition of e and g and the cavity in vacuum, the atom ends up in g, leaving in the cavity a superposition of the zero and one photon Fock states:

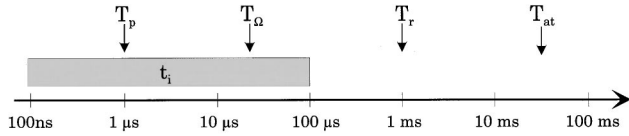$$(c_e|e\rangle + c_g|g\rangle)|0\rangle \mapsto |g\rangle(c_e|1\rangle + c_g|0\rangle).$$
(3.6)

FIG. 4. Relevant times of a CQED experiment, plotted on a logarithmic scale. T_{at}, T_r, T_Ω, t_i, and T_p are defined in the text. t_i can be varied in the range depicted by the gray bar.

The reverse transformation, obtained for an atom initially in g interacting with a field in a coherent superposition of 0 and 1 photon Fock states, is

$$(c_1|1\rangle + c_0|0\rangle)|g\rangle \mapsto |0\rangle(-c_1|e\rangle + c_0|g\rangle). \qquad (3.7)$$

The "π Rabi rotation" thus maps the state of one system onto the other. This mapping can be used to prepare or to detect the cavity field in an arbitrary superposition of 0 and 1 photon states.

When $\Omega t_i = 2\pi$, the atom-field system evolves according to

$$|e,0\rangle \mapsto -|e,0\rangle, \quad |g,1\rangle \mapsto -|g,1\rangle. \qquad (3.8)$$

After a full cycle of Rabi oscillation, the atom-cavity system experiences a global quantum phase shift π. Similar phase shifts are obtained for a spin-1/2 system undergoing a 2π rotation in ordinary space (Rauch *et al.*, 1975; Werner *et al.*, 1975). Note that this 2π rotation also plays a central role in the micromaser trapping states (Weindinger *et al.*, 1999). Since $|g,0\rangle$ is not affected by the atom-field coupling, the phase shift experienced by an atom entering C in g is conditioned to the presence of a photon inside the cavity. This conditional dynamics is, as we will see, essential for realizing a quantum phase gate.

The $\pi/2$, π, and 2π Rabi pulses combined with classical Ramsey ones provide the basic ingredients of our entanglement "recipe." In general, the atomic velocity v is chosen to produce a 2π Rabi rotation for a full crossing of the cavity mode ($v = 503$ m/s). By applying an electric field across the cavity mirrors at appropriate times, the $e \Leftrightarrow g$ transition can be abruptly tuned out of resonance, freezing from then on the atom-cavity evolution. In this way, we can adjust t_i to the values corresponding to π and $\pi/2$ Rabi pulses. We can then combine, on a sequence of atoms crossing the cavity with the same velocity v, entanglement production by a $\pi/2$ rotation, state transfer by a π rotation and conditional dynamics by a 2π rotation, engineering in this way complex entangled states.

These manipulations rely on an accurate timing of operations on different atoms. These are possible only because the various relevant times of the experiment are properly ordered, as indicated in Fig. 4. We have plotted there, on a logarithmic scale, the typical circular level lifetime T_{at}, the cavity damping time T_r, the Rabi period $T_\Omega = 2\pi/\Omega$, and the typical Ramsey pulse duration $T_p = 1$ μs. The effective atom-cavity interaction time t_i can be varied between the time resolution of our timing unit (100 ns) and about 100 μs (atoms with a velocity of 100 m/s interacting resonantly with the mode during its

full cavity crossing time). It is essential for these experiments that the relaxation times T_{at} and T_r are much longer than T_Ω (strong-coupling regime). It is also important that the time step resolution is much smaller than T_Ω.

C. Quantum Rabi oscillation in an applied field

Atom-field entanglement is also produced when the atom interacts with a cavity field in the n-photon Fock state. For example, the system starting from the initial state $|e,n\rangle$ evolves into

$$|\Psi_{e,n}(t_i)\rangle = \cos(\Omega\sqrt{n+1}\,t_i/2)|e,n\rangle$$
$$+ \sin(\Omega\sqrt{n+1}\,t_i/2)|g,n+1\rangle. \qquad (3.9)$$

The maximally entangled EPR state is produced in a time $\pi/2\Omega\sqrt{n+1}$, faster than in the zero photon case. Note that Rabi oscillations induced by pure Fock states of the field up to $n=2$ have been recently observed (Varcoe, Brattke, and Walther, 2000).

Fock states are generally difficult to generate, but one can easily observe the evolution of an atom interacting with a small coherent field $|\alpha\rangle = \Sigma_n c_n |n\rangle$, where $c_n = \exp(-|\alpha|^2/2)\alpha^n/\sqrt{n!}$. The quantum Rabi oscillation signal appears now as a sum of sinusoidal terms at frequencies $\Omega\sqrt{n+1}$, weighted by the probabilities $|c_n|^2$ for finding the corresponding photon number in the coherent field:

$$P_e = \sum_n |c_n|^2 \frac{1 + \cos\Omega\sqrt{n+1}\,t_i}{2}. \qquad (3.10)$$

The corresponding experimental signal is shown in Fig. 5(a) for an initial coherent field containing 0.85 photons on the average. We observe an oscillation collapse due to the dispersion of the Rabi frequencies and a subsequent "revival" (Eberly *et al.*, 1980) when the terms oscillating at different discrete frequencies come back into phase. The signal is damped by various imperfections. This signal provides direct evidence of field energy quantization. The field amplitude distribution is revealed by the frequency spectrum of the Rabi signal. This spectrum, obtained by a Fourier transform, is plotted in Fig. 5(b). It exhibits well separated discrete frequency components scaling as the square roots of the successive integers.

IV. CREATION OF AN EPR PAIR

In the simplest entanglement experiment (Hagley *et al.*, 1997), we let an atom A_1 undergo a $\pi/2$ Rabi rotation in an initially empty cavity. The resulting atom-cavity state is the EPR pair described by Eq. (3.5). This entanglement persists after A_1 has left C. Detecting at some distance downstream the atom in a given quantum state instantaneously collapses the cavity mode in the correlated field state. For example, detecting the atom in level e (respectively, g) amounts to preparing a zero (one) photon Fock state in the cavity (Maître *et al.*,
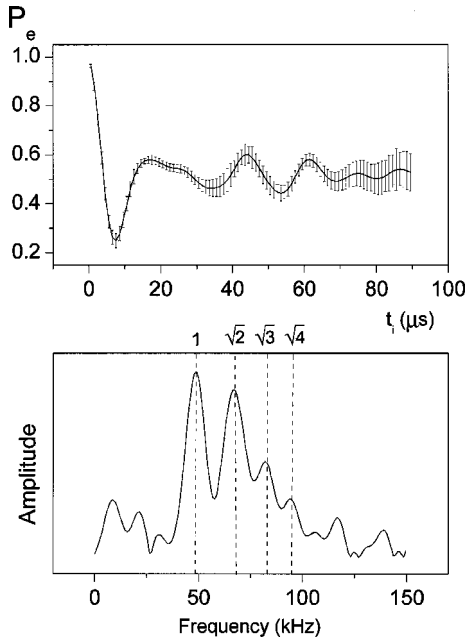
FIG. 5. Quantum Rabi oscillation in a coherent field. The cavity contains initially a coherent field with 0.85 photons on the average. (a) Probability P_e for finding the atom in the initial state e as a function of the effective interaction time t_i. (b) Fourier transform of the signal in (a) revealing the discrete Rabi frequencies, occurring at the successive square roots of the integers.

FIG. 6. Temporal sequence of the EPR pair preparation. Space lines of A_1, A_2, and C in a position versus time diagram. The black diamonds indicate a resonant Rabi rotation (with the angle as a label). The open squares represent the detection events. The gray circles represent classical Ramsey pulses. (a) Timing of the EPR state preparation with a direct measurement of energy anticorrelations. (b) Timing of the transverse correlation experiment.

1997). One can also, by detecting linear superpositions of e and g states (using a R_2^{eg} mixing pulse on the $e \Leftrightarrow g$ transition in front of the detector D), project the field onto corresponding superpositions of 0 and 1 Fock states. Contrary to photon-number states, such superpositions have a nonzero electric field expectation value, i.e., a nonuniform phase distribution. The phase information contained in the classical R_2^{eg} field has been transferred to the quantum cavity mode, via the atomic measurement and the nonlocal quantum correlations.

In order to read out the field state, we need a second atom A_2, prepared in g and undergoing a π Rabi rotation in a single photon field. This atom carries away the cavity state including its entanglement with A_1. In other words, detecting the $A_1 - C$ entanglement is equivalent to performing an $A_1 - A_2$ two-atom EPR experiment. After A_2 has crossed C, the cavity is empty and disentangles from the atomic pair, which ends up in state

$$|\Psi_{Pair}\rangle = \frac{1}{\sqrt{2}}(|e_1, g_2\rangle - |g_1, e_2\rangle), \qquad (4.1)$$

where the subscripts refer to the atom number. Since e and g represent, respectively, the $|+\rangle$ and $|-\rangle$ pseudospin states, $|\Psi_{Pair}\rangle$ appears as the rotation invariant spin singlet state. The temporal sequence of this EPR atomic pair preparation is schematized in Fig. 6(a). It exhibits the space lines of the two atoms and of the cavity mode in a qualitative position-versus-time diagram. The Rabi rotations and detection events are indicated by symbols (see figure caption).
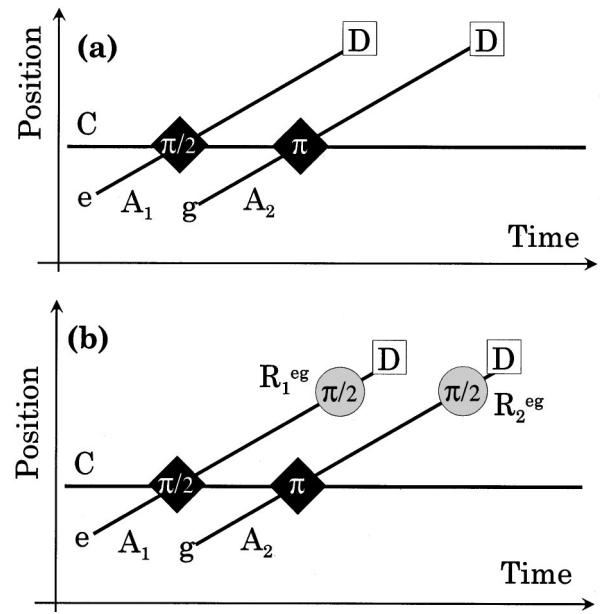
In order to check the atomic entanglement, we have shown that the measurements of the two spins along an arbitrary direction are anticorrelated. In a first experiment, we directly check the anticorrelations of the atomic energies, corresponding to a measurement along the Oz axis [see Fig. 6(a)]. We obtain, for the four possible detection channels, the probabilities $P_{eg} = 0.44$, $P_{ge} = 0.27$, $P_{gg} = 0.23$, $P_{ee} = 0.06$, with statistical errors of the order of 0.03. For a pure EPR pair, these probabilities should be $P_{eg} = P_{ge} = 1/2$, $P_{ee} = P_{gg} = 0$. Several experimental imperfections discussed by Hagley *et al.* (1997) account for the differences.

We have also checked "transverse" spin component correlations, exhibiting the phase information transfer between the two atoms mediated by the nonlocal correlations. We make use of Ramsey $\pi/2$ pulses R_1^{eg} and R_2^{eg} applied, respectively, on atoms A_1 and A_2 on the $e \Leftrightarrow g$ transition after they have left C. The timing of this experiment is depicted in Fig. 6(b) (the gray circles represent these classical pulses). The correlations between the two atomic detections are exhibited by plotting, versus the relative phase ϕ between the two Ramsey pulses, the "Bell signal"[3] $\langle \sigma_{x,1} \sigma_{\phi,2} \rangle = P_{g_1,g_2} + P_{e_1,e_2} - P_{g_1,e_2} - P_{e_1,g_2}$, where the σ's are Pauli matrices associated with the pseudospins and P_{a_1,b_2} is the probability for

---

[3]This atomic correlation signal is similar to the photon polarization correlations used for experimental tests of Bell inequalities.
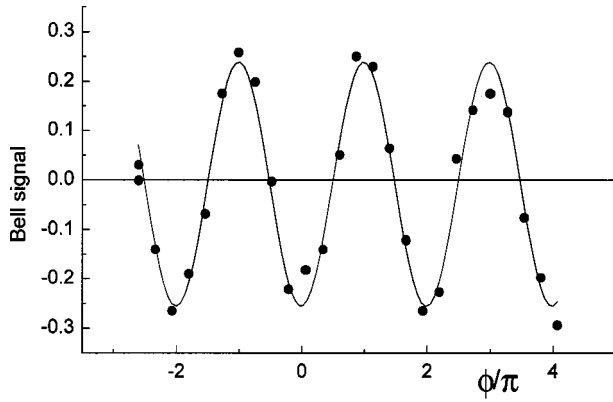
FIG. 7. "Bell signal" plotted versus the relative phase ϕ (in units of π) of pulses R_1^{eg} and R_2^{eg}. The line is a sine fit.

detecting A_1 in a and A_2 in b ($\{a,b\}=\{g,e\}$). This correlation should be ideally equal to -1 ($+1$) for $\phi=0$ ($\phi=\pi$) (perfect anticorrelation for a detection of the two particles along the same direction).

Figure 7 presents the corresponding experimental data. The contrast reduction is due both to the limited purity of the EPR state and to imperfections of the Ramsey pulses. Note that we are performing here a kind of Ramsey interferometry. We apply, however, the two pulses on different atoms. The observation of fringes in this case shows that the pair of atoms behaves as a single system sharing quantum coherences.

The Bell signal contrast in this experiment is not high enough to observe a violation of the Bell inequalities (Bell, 1964). In comparison with the experiments with photons (Aspect, Dalibard, and Roger, 1982; Zeilinger, 1998), the quality of our Ramsey spin "analyzers" is too low. Improvements of the setup, briefly described in Sec. IX, will hopefully allow us to improve the situation, opening the way to a new type of Bell inequality experiment with massive particles. A similar experiment has recently been performed with entangled ions (Rowe *et al.*, 2001).

V. THE QUANTUM PHASE GATE

The conditional dynamics induced by the 2π Rabi rotation [Eq. (3.8)] realizes an elementary quantum logic gate which can be used to entangle qubits in a "programmed" process. Let us consider an atom crossing the cavity, containing zero or one photon. The atom is either in the resonant state g or in the "spectator" state i (far off resonance and thus not affected by the cavity interaction). If C is empty or if the atom is in i, the global state is unchanged. However, if the atom is in g and the cavity in $|1\rangle$, the global state undergoes the transformation $|g,1\rangle\mapsto\exp(i\Phi)|g,1\rangle$ with $\Phi=\pi$ [see Eq. (3.8)]. This is the conditional dynamics of a "quantum phase gate" (Monroe *et al.*, 1995). This gate does not modify the photon number in the cavity.

If the atom enters in a coherent superposition of g and i (amplitudes c_g and c_i), the gate performs the transformations

$$(c_g|g\rangle+c_i|i\rangle)|0\rangle\mapsto(c_g|g\rangle+c_i|i\rangle)|0\rangle,$$

$$(c_g|g\rangle+c_i|i\rangle)|1\rangle\mapsto(e^{i\Phi}c_g|g\rangle+c_i|i\rangle)|1\rangle. \quad (5.1)$$

The superposition is unchanged if the cavity is empty, while the phase of the atomic coherence is shifted by $\Phi=\pi$ when the cavity contains one photon. If the field is now in a superposition of zero and one photon states (amplitudes c_0 and c_1,), we have

$$|i\rangle(c_0|0\rangle+c_1|1\rangle)\mapsto|i\rangle(c_0|0\rangle+c_1|1\rangle),$$

$$|g\rangle(c_0|0\rangle+c_1|1\rangle)\mapsto|g\rangle(c_0|0\rangle+e^{i\Phi}c_1|1\rangle). \quad (5.2)$$

The phase of the field coherence is shifted by Φ by an atom in g, while it is unchanged by an atom in i. Finally, it is easy to see that, when both qubits are in state superpositions, the gate generates atom-cavity entanglement.

We have proved the coherent gate operation by performing two complementary experiments checking these transformations. To study the transformation described by Eq. (5.1), we either leave initially the cavity in the zero photon state or prepare it in the one photon state by using the π Rabi pulse operation on a first "source" atom A_1 initially prepared in e (see Sec. IV). We then send a second atom A_2, initially in g, prepared in a superposition with equal weights of g and i($c_g=c_i$ $=1/\sqrt{2}$) by a Ramsey pulse R_1^{gi}. This atom undergoes a full 2π Rabi rotation in C. We probe the atomic coherence by applying another $\pi/2$ Ramsey pulse R_2^{gi} before the detection in D. The timing of the experiment corresponding to the one photon case is schematized on Fig. 8(a). In the zero photon case, atom A_1 is removed.

The Ramsey fringes observed on atom A_2 submitted to the R_1^{gi} and R_2^{gi} pulses are shown on Fig. 9, as open diamonds (when the zero photon state is initially prepared in C) and by black squares (when the cavity initially contains one photon). We observe clearly the π phase shift of the atomic coherence induced by the presence of one photon.

The complementary experiment testing Eq. (5.2) involves a coherent superposition of 0 and 1 photon states. It is prepared by injecting in C a small coherent field $|\alpha\rangle=c_0|0\rangle+c_1|1\rangle+\Sigma_{n>1}c_n|n\rangle$ (Glauber, 1963). When the average photon number $|\alpha|^2$ is low (about 0.1), the c_n coefficients are negligible for $n>1$ and, to a good approximation, $|\alpha\rangle\simeq c_0|0\rangle+c_1|1\rangle$, with $c_1\simeq\alpha$. We then send atom A_2, prepared in a coherent superposition of g and i by a Ramsey $\pi/2$ pulse R_1^{gi}, and submit this atom to a 2π Rabi rotation in C (note that the R_2^{gi} pulse and atom A_1 are not used in this experiment). When A_2 is detected in i, the field phase should be unchanged. When A_2 is detected in g, the field state in C becomes $c_0|0\rangle+c_1\exp(i\Phi)|1\rangle\simeq|\exp(i\Phi)\alpha\rangle=|-\alpha\rangle$. The classical phase of the coherent field is thus π shifted.

To detect this shift, we analyze the field phase by a "homodyning" method: we inject, after A_2 has left C, a field with the amplitude $\alpha\exp(i\theta)$. It adds coherently to the field already present in C. The phase $\theta=T\Delta$ depends upon the detuning Δ between S and C ($T=100\,\mu$s is the delay between the two field injections).
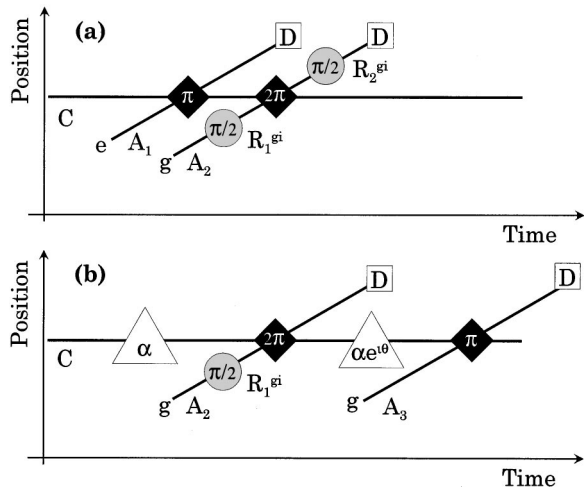
FIG. 8. Timing of the quantum phase gate experiment. Same conventions as in Fig. 6. (a) Check of the atomic coherence phase shift. A single photon state is prepared in C by atom A_1. (b) Check of the field phase shift. The triangles represent coherent field injection in the cavity mode [amplitudes α and $\alpha \exp(i\theta)$].

The amplitude of the resulting field ideally varies between 0 and 2α as a function of θ. The final field is probed by sending an atom A_3, initially in g, across C. It undergoes a π-Rabi pulse in the field of 1 photon. Hence the probability P_{e_3} for detecting A_3 in e is ideally equal to the probability for finding a single photon in C. This probability is approximately equal to the average photon number. The timing of this experiment is depicted on Fig. 8(b). The two field injections in the cavity mode are schematized by triangles on the cavity space-time line.

Figure 10 shows, versus θ, the conditional probabilities $P(e_3/i_2)$ and $P(e_3/g_2)$ for finding the probe A_3 in e provided A_2 was found in i (circles) or in g (diamonds). The lines are obtained by a simple model which accounts for the experimental imperfections by adjustable
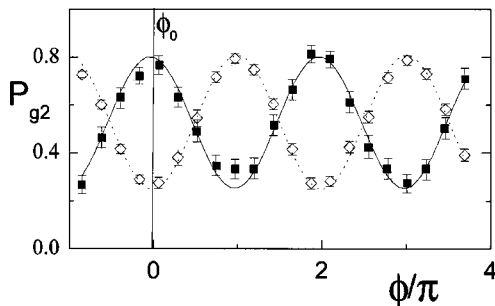

FIG. 9. Test of the atomic coherence phase shift. Probability P_{g_2} for detecting atom A_2 in state g versus the phase ϕ of the Ramsey interferometer (units of π). Open diamonds: empty cavity. Solid squares: cavity containing one photon. The error bars reflect the statistical variance. The lines are sine fits. For phase $\phi_0 = 0$, indicated by a vertical line, the atomic state is directly correlated to the photon number (i for zero photon, g for one photon)
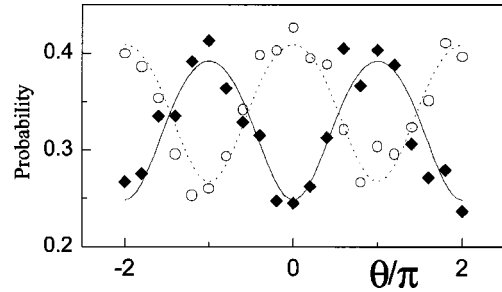
FIG. 10. Test of the field phase shift. Conditional probabilities $P(e_3/i_2)$ (circles) and $P(e_3/g_2)$ (diamonds) versus θ (units of π) for detecting A_3 in e if A_2 has crossed C in i or g. Points are experimental and lines are fits based on a simple model.

contrasts and offsets. The modulation in these signals reflects the interference of the two field pulses. When A_2 is detected in i, the probe absorption is minimum for $\theta = \pm\pi$ since the amplitudes of the two injected fields then add with opposite phases. When, instead, A_2 is detected in g, the probe absorption becomes minimum for $\theta = 0$, which exhibits clearly the π phase shift produced by atom A_2 in this case.

The data of Figs. 9 and 10 demonstrate clearly the two complementary aspects of the quantum phase gate, expressed by Eqs. (5.1) and (5.2). Note that the phase Φ can be tuned over the complete $0,2\pi$ range by adjusting the atom-cavity detuning (Rauschenbeutel *et al.*, 1999).

VI. ABSORPTION-FREE DETECTION OF A SINGLE PHOTON

The quantum phase gate, sandwiched between two $\pi/2$ Ramsey pulses, realizes a "control-not" gate[4] which can be used to detect a single photon without absorbing it. A simple inspection of the signal in Fig. 9 shows that, at a fringe extremum (phase $\phi_0 = 0$ depicted by a vertical line), the final atomic state is correlated to the photon number. In an ideal experiment, the atom exits in i if the cavity is empty, in g if C contains one photon. The atom appears as a microscopic measuring device, carrying away information about the photon number. This field intensity measurement does not change the photon number. Note that the question whether the photon left in C is the same as—or a copy of—the original one has no meaning in quantum mechanics since photons in a field mode are indiscernible. The only pertinent notion is the cavity quantum state, which remains unchanged if it is in a one-photon Fock state. This measurement is an absorption-free or "quantum nondemolition" (QND) one, provided the field is in the $\{|0\rangle, |1\rangle\}$ subspace. Out of this subspace, the 2π Rabi rotation condition is not fulfilled for all photon numbers n (because of the $\sqrt{n+1}$ dependence of the Rabi frequency—see Sec. III). This

---

[4]In this gate, one of the qubits, the "control," conditions, depending on its state, the evolution of the other, the "target." The latter switches state when the control is in state $|1\rangle$ and remains unchanged when the control is in state $|0\rangle$.

method thus amounts to a single photon QND detection (SP-QND) (Nogues *et al.*, 1999).

Quantum nondemolition measurements have been proposed in the 1970s to improve the sensitivity of position or velocity measurements in gravitational wave detectors (Braginsky, Vorontsov, and Khalili, 1977; Braginsky and Khalili, 1992). A QND measurement realizes basically the ideal quantum-measurement presented in quantum-mechanics textbooks (Caves *et al.*, 1980). It gives as a result one of the eigenvalues of the measured observable and projects the measured system on the corresponding eigenstate. Provided it is also an eigenstate of the free Hamiltonian, there is no evolution after the measurement. Subsequent QND measurements give the same result again and again. Any difference between two consecutive measurements provides thus a very sensitive probe of a perturbation acting between them. Most realistic particle measurements in physics (including photon counting) are far from realizing these ideal conditions. Usually in photodetection, for instance, the photon is absorbed by a photosensitive surface. A QND detector for light must be perfectly transparent. Although this may appear a strange property, it is, as this experiment shows, compatible with quantum laws.

In fact, QND measurements have been widely studied in quantum optics (Grangier, Levenson, and Poizat, 1998). Most experiments so far have involved the interaction of a "signal" beam with a weak "meter" beam. Both beams travel together in a nonlinear transparent medium [such as a nonlinear crystal (La Porta *et al.*, 1989), an atomic vapor close to a resonance line (Roch *et al.*, 1997), or an optical fiber (Levenson *et al.*, 1986)]. The meter experiences an index of refraction change proportional to the signal light beam intensity. This index reflects directly on the meter beam phase at the exit of the medium, which is read out by comparison with a phase reference in an interferometric arrangement. At the output of the interferometer, the meter's intensity fluctuations directly reveal the signal ones. The signal intensity is not modified. The phase of the signal beam, however, is affected by the index changes due to the quantum fluctuations of the meter beam. In an ideal QND determination of the photon number, the signal phase is completely blurred.

In a variety of experimental conditions, the quantum correlations between the signal and meter have been demonstrated and improved over the years (Grangier, Levenson, and Poizat, 1998). Repeated measurements have also been performed, exhibiting the essential properties of QND schemes (Bencheick *et al.*, 1995; Bruckmeier *et al.*, 1997). All of these experiments, relying on nonlinear optical effects, operate only on macroscopic propagating laser beams, involving a very large number of photons.

Our SP-QND scheme bears strong analogies with these experiments. The signal is the single photon stored in the cavity. The meter is the circular atom, whose output phase is read by the Ramsey interferometer. The nonlinear interaction is the 2π Rabi rotation. The extremely strong coupling of circular Rydberg atoms with

millimeter-wave radiation makes it possible to push the QND principle down to the single photon level (Nogues *et al.*, 1999). Note that, as in other QND schemes, the SP-QND detection destroys phase information. If the field is initially in a superposition of zero and one photon states, the measurement reduces it to a Fock state, in which the phase information is completely lost. Note also that the average field energy is changed in an individual measurement. This is not surprising since this measurement pins down the energy of a system initially presenting energy fluctuations.

In order to demonstrate the nondestructive feature of the SP-QND scheme, we have also realized repeated photon detections, either two successive QND detections, or one QND detection followed by an absorptive measurement. We will only describe the latter experiment, whose timing is depicted in Fig. 11. We have performed the QND measurement on a small 0.25 photon thermal field building up after the cooling procedure, in which the probability for having more than one photon is small. We send atom A_1 to implement the SP-QND measurement. We then remeasure the cavity state by an absorptive measurement. A probe atom A_2 is sent in state g and undergoes a π pulse in a single photon field. It thus exits in level e if the cavity contained one photon after the first measurement.

The results of this experiment are shown in Fig. 12. Repeating the double measurement sequence many times, we have plotted versus the phase ϕ of the Ramsey interferometer the conditional probabilities $P(e_2/g_1)$ (squares) and $P(e_2/i_1)$ (diamonds) for detecting A_2 in e provided the SP-QND atom A_1 has been detected in i or g. We have also plotted, as a reference, the probability $P(e_2)$ for finding A_2 in e when no SP-QND atom A_1 is sent (triangles), i.e., the results of a simple absorptive measurement of the initial thermal field.

The modulations of the absorption rates $P(e_2/g_1)$ and $P(e_2/i_1)$ reveal the field modifications due to the SP-QND measurement performed by A_1. Let us focus, for example, on the particular case $\phi = 0$. Atom A_1 indicates one photon when detected in g, zero photon when detected in i. In an ideal experiment, the field is then projected onto the corresponding state. A_2 should thus absorb a photon and be detected in e if A_1 is detected in g. We observe effectively that the probability $P(e_2/g_1)$ is larger than P_{e_2} for this phase setting. The *a posteriori*
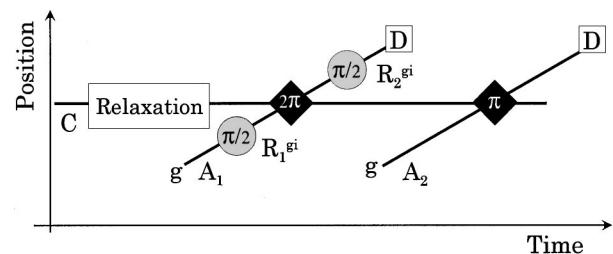

FIG. 11. Timing of repeated measurement of a single photon: QND measurement of a thermal field followed by an absorptive one. Cavity relaxation after the cooling procedure builds up an initial 0.25 photon field.
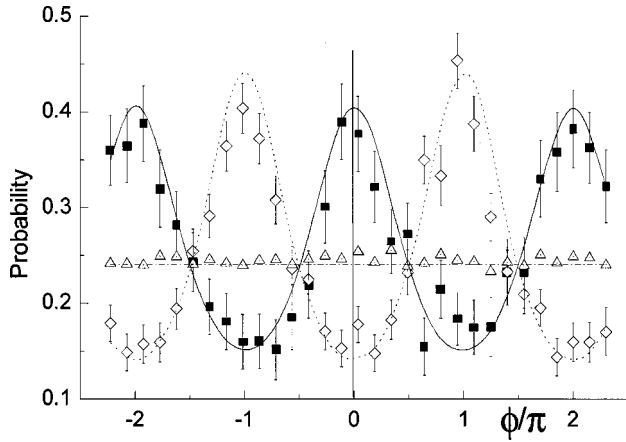
FIG. 12. Repeated thermal field measurement. Square and diamond experimental points show the conditional probabilities $P(e_2/g_1)$ and $P(e_2/i_1)$ for finding the second atom in e, provided the first one has been measured in g or i, versus the Ramsey interferometer phase ϕ. The lines are obtained by numerical simulations. The triangles correspond to the probability $P(e_2)$ for finding A_2 in e when no A_1 atom is sent. The phase $\phi_0 = 0$ is indicated by a vertical line.

probability for having one photon after the SP-QND measurement is higher than the *a priori* one if A_1 is detected in g. This reveals the nonabsorptive nature of the measurement and exhibits its repeatability. When the SP-QND atom A_1 is detected in i, the conclusions are reversed and the probability for getting A_2 in e is lower than the *a priori* one. Note also that, for phase $\phi = \pi/2$, the three probabilities $P(e_2)$, $P(e_2/g_1)$, and $P(e_2/i_1)$ are the same. For this phase, A_1 is always detected with a 50% probability in i or g. It does not convey any information on the field intensity and its detection does not modify the field state. Note that the sum of the $P(e_2/g_1)$ and $P(e_2/i_1)$ signals weighted by the probabilities for finding A_1 in g or i, respectively, which represents the mean photon number in the thermal field, is equal to $P(e_2)$, as required by ideal measurement theory.

The observed conditional probabilities do not reach the ideal zero and one values due to various experimental imperfections (Nogues *et al.*, 1999). By performing a careful analysis of such signals, we have made a quantitative determination of the efficiency of our QND scheme. It allows one to tell, with an 80% success rate, whether there is zero or one photon in C immediately after the passage of the meter atom. The probability that this atom has absorbed the photon, due to the imperfection of the 2π Rabi pulse, is about 10%.

VII. ENGINEERED ENTANGLEMENT OF THREE QUANTUM SYSTEMS

The quantum phase gate, which does not affect the photon number in C, can, in principle, be used to entangle an arbitrary number of atoms with the field. We made a first step in this direction by preparing an entangled state of three particles (Rauschenbeutel *et al.*,

2000). We prepare a maximally entangled state of the GHZ type by operating a quantum phase gate on an atom-cavity EPR pair. The sequence of operations could be modified to produce an arbitrary entangled state.

The entangled state preparation timing is shown in Fig. 13(a). We send across C, initially empty, a first atom A_1 initially in e. It undergoes in C a $\pi/2$ Rabi rotation. The $A_1 - C$ EPR state is then given by Eq. (3.5). A second atom A_2, initially in g, is prepared, before C, in $(|g\rangle + |i\rangle)/\sqrt{2}$ by a Ramsey pulse P_2^{gi}. This atom undergoes a 2π Rabi rotation in C, and thus performs a quantum phase gate operation with the cavity field as the control qubit. If C contains one photon, the A_2 coherence is phase shifted by π. It stays unchanged if C is empty. The resulting $A_1 - A_2 - C$ quantum state is

$$|\Psi_{triplet}\rangle = \frac{1}{2}[|e_1\rangle(|i_2\rangle + |g_2\rangle)|0\rangle$$
$$+ |g_1\rangle(|i_2\rangle - |g_2\rangle)|1\rangle]. \tag{7.1}$$

This three-particle entangled state can be rewritten as

$$|\Psi_{triplet}\rangle = \frac{1}{2}[|i_2\rangle(|e_1,0\rangle + |g_1,1\rangle)$$
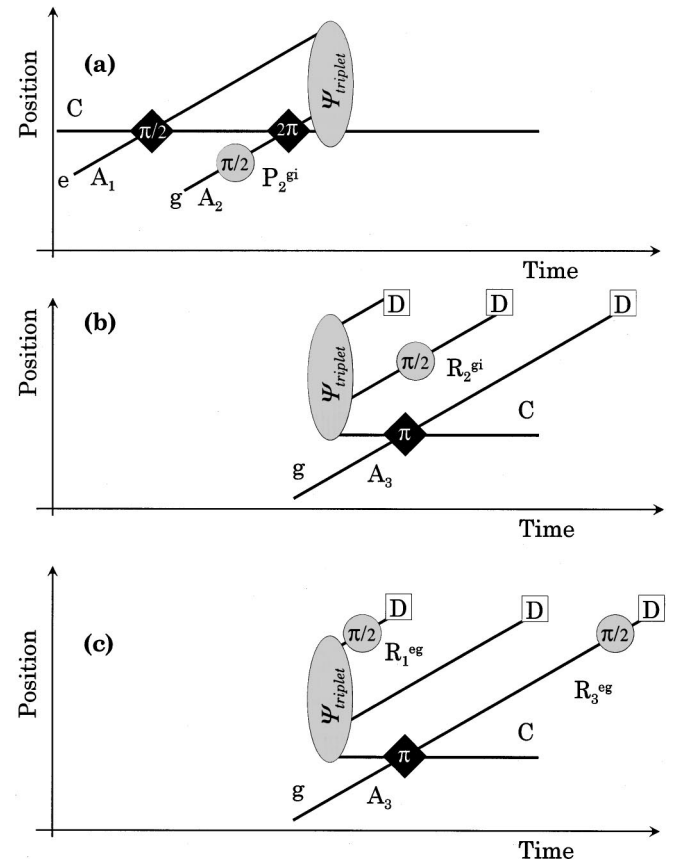$$+ |g_2\rangle(|e_1,0\rangle - |g_1,1\rangle)], \tag{7.2}$$

FIG. 13. Timing of the three particle entanglement. (a) State preparation. (b) Test of "longitudinal" correlations. (c) Test of "transverse" correlations. Reprinted with permission from Rauschenbeutel *et al.* (2000). (Copyright 2000, American Association for the Advancement of Science.)

describing an atom A_2 entangled with an $A_1 - C$ EPR pair, whose phase is conditioned to the A_2 state. Defining the pseudospin states $|+_i\rangle$ $(|-_i\rangle)$ (with $i=1,2$) as $|+_1\rangle = |e_1\rangle$ $(|-_1\rangle = |g_1\rangle)$, $|\pm_2\rangle = (|g_2\rangle \pm |i_2\rangle)/\sqrt{2}$, and $|+_C\rangle = |0\rangle$ $(|-_C\rangle = |1\rangle)$, $|\Psi_{triplet}\rangle$ takes the form of the GHZ three spin state:

$$|\Psi_{triplet}\rangle = \frac{1}{\sqrt{2}}(|+_1,+_2,+_C\rangle - |-_1,-_2,-_C\rangle). \quad (7.3)$$

In order to check the $A_1 - A_2 - C$ entanglement, we copy the state of C onto a third atom A_3, prepared in g and undergoing a π Rabi rotation in a single photon field. Within a phase, A_3 maps exactly the state of C, and the two atoms plus cavity correlations correspond directly to the three-atom correlations.

As in the analysis of the EPR pair (see Sec. IV), two sets of measurements in two orthogonal bases are required in order to characterize the three-particle entanglement. In a first experiment [experiment I, see timing in Fig. 13(b)], we test "longitudinal" correlations by detecting the three atomic pseudospins along the Oz quantization axis. Atoms A_1 and A_3 are directly detected. For A_2, the $|+_2\rangle$ and $|-_2\rangle$ states (linear combinations of i and g) are mapped onto i and g, respectively, by a $\pi/2$ Ramsey pulse R_2^{gi}. Note that the complete sequence for A_2 amounts to a SP-QND determination of the field intensity. The three atoms should thus be detected in $\{e_1,i_2,g_3\}$ or $\{g_1,g_2,e_3\}$, with equal probabilities. Figure 14 presents the observed detection probabilities for the eight relevant channels. The longitudinal correlations (black bars) are clearly observed. The other channels (white bars) correspond to spurious effects.

These correlations, taken alone, could be explained classically as a statistical mixture involving mainly $|e_1,i_2,g_3\rangle$ and $|g_1,g_2,e_3\rangle$. To exhibit the quantum coherence of the three-particle state superposition, we check, in experiment II, "transverse" pseudospin correlations. The corresponding timing is schematized in Fig. 13(c). A_2 is detected directly along the pseudo-Oz direction (atom found in g or i). A_1 is detected along the Ox axis, and A_3 along an axis in the horizontal plane making an angle ϕ with the Ox axis. For these detections, we use the Ramsey pulses R_1^{eg} and R_3^{eg}, with a ϕ phase difference. We finally measure the Bell signal correlation $\langle \sigma_{x,1}\sigma_{\phi,3}\rangle$ conditioned by the final A_2 state. As a reference signal, we also record the $A_1 - A_3$ Bell signal without sending the quantum phase gate atom A_2.

These signals are shown in Fig. 15. The reference signal (diamonds) exhibits the EPR correlations discussed in Sec. IV. The $A_1 - A_3$ correlation when A_2 is sent and detected in i and g are represented by circles and squares, respectively. In the first case, the phase of the $A_1 - A_3$ EPR correlation is not changed whereas it is phase shifted by π in the second case. This shows that the phase of the EPR pair is controlled by the quantum phase gate atom [see Eq. (7.2)].

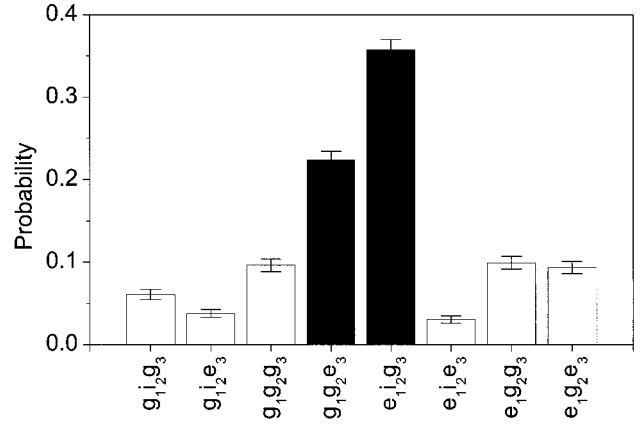The combined results of experiments I and II prove the entanglement of the three quantum systems. From

FIG. 14. Longitudinal correlations (experiment I). Histograms of the detection probabilities for the eight relevant detection channels. The two expected channels (g_1,g_2,e_3 and e_1,i_2,g_3) (in black) clearly dominate the others (in white), populated by spurious processes. The error bars are statistical. Reprinted with permission from Rauschenbeutel *et al.* (2000). (Copyright 2000, American Association for the Advancement of Science.)

the analysis of the data, we infer that the GHZ state is prepared with a fidelity of 54% (Rauschenbeutel *et al.*, 2000). This experiment is the first one in which a controlled, tailorable entanglement has been produced between three individually addressed particles. It opens interesting perspectives on the realization of stringent tests of quantum nonlocality.

VIII. NONRESONANT ENTANGLEMENT

A. Single atom index effect and Schrödinger cat states

Let us now consider the situation where the cavity mode is slightly detuned from the $e \to g$ transition frequency (level i does not play any role here). The atom-cavity frequency mismatch δ is greater than the vacuum Rabi frequency Ω. Since energy can no longer be conserved during elementary photon absorption and emis-
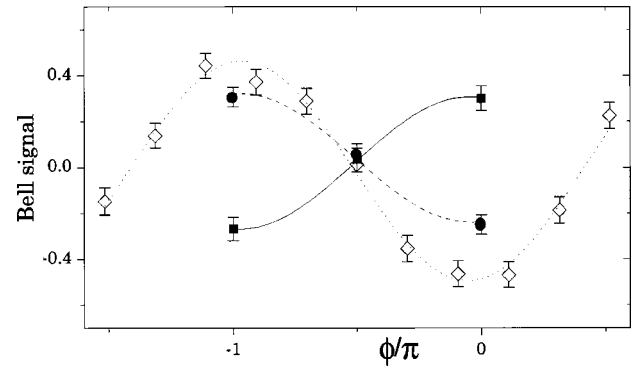

FIG. 15. Transverse correlations (experiment II). Bell signal versus ϕ. Open diamonds: no A_2 atom. Solid circles: atom A_2 detected in i. Solid squares: atom A_2 detected in g. Error bars are statistical. Lines are sine fits. Reprinted with permission from Rauschenbeutel *et al.* (2000). (Copyright 2000, American Association for the Advancement of Science.)

sion processes, the atom and the field cannot get entangled through resonant energy exchange. This does not mean, however, that the two subsystems do not interact. The mere presence of an atom in the cavity slightly shifts its frequency. This is a refractive index effect, produced by a single atom (Haroche and Raimond, 1994). This effect depends upon the atom's energy state. When the cavity mode frequency is larger than the atomic transition one, the field frequency is increased or decreased, by an amount $\pm\Omega^2/4\delta$ depending upon whether the atom is in level g or e. When the atom crosses the cavity in a linear superposition of these levels, the cavity mode is then in a superposition of states corresponding to two different frequencies at once. This peculiar situation leads to the possibility of studying new kinds of entanglement between a microscopic system (the atom) and a mesoscopic field in the cavity (Brune *et al.*, 1996). These experiments are very briefly described here in qualitative terms.

Let us start by injecting in C, using source S, a small coherent field, with a classical amplitude α. This field decays within the cavity damping time T_r. Note that this experiment was realized with a cavity without ring. The photon storage time was 160 μs only. We send then an atom A_1 across C. The period of the field oscillations is slightly modified as the atom interacts with the field mode. This results in a kick of the field phase, after the atom has left C. Equivalently, the vector representing the field rotates in phase space by an angle $\pm\Phi = \pm\Omega^2 t_e/4\delta$, depending on the state of the atom, where t_e is the effective interaction time. If the atom is sent in the linear superposition $(|e\rangle+|g\rangle)/\sqrt{2}$, the combined atom-field system evolves into an entangled state which may be written as

$$\frac{1}{\sqrt{2}}(e^{i\Phi}|e,\alpha e^{i\Phi}\rangle+|g,\alpha e^{-i\Phi}\rangle), \qquad (8.1)$$

where $|e,\alpha e^{i\Phi}\rangle$ ($|g,\alpha e^{-i\Phi}\rangle$) represent, respectively, the atom in level e (g) correlated with the field in the coherent state with complex amplitude $\alpha e^{i\Phi}$ ($\alpha e^{-i\Phi}$). The situation is reminiscent of the famous Schrödinger cat (Schrödinger, 1935) entangled with a single atom in a superposition of states corresponding to its "live" and "dead" states. We note that the vector describing the classical complex field amplitude in the Fresnel plane acts here as a kind of "meter" pointing in two different directions correlated to the atom's energy. In other words, the field plays the role of an apparatus measuring the atom's energy in a quantum nondemolition way. The situation is symmetric to the one described above (in which an atom is used to measure nondestructively the field's energy, see Sec. VI).

B. A complementarity experiment

This leads us to an experiment demonstrating in a simple way the complementarity principle. The Ramsey fringes observed when the atom undergoes two $\pi/2$ microwave pulses resonant with the $e\Leftrightarrow g$ transition in R_1^{eg}
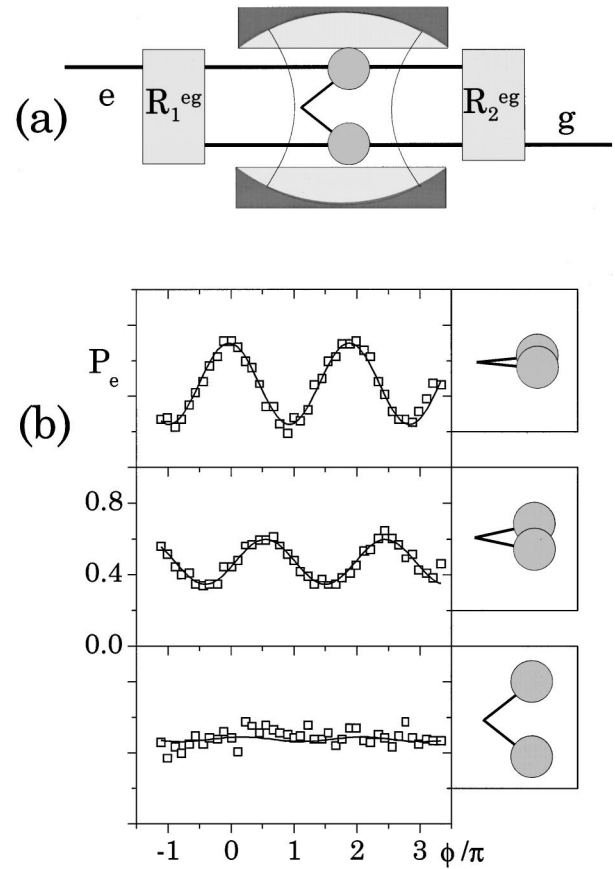

FIG. 16. Complementarity experiment: (a) Principle of the experiment: an atom follows two interfering paths between the Ramsey zones, and the phase of the field stored in the cavity provides a "which path" information. The two coherent components of the field are pictorially represented by a vector in the Fresnel plane. A small uncertainty circle on the tip of this vector depicts the field amplitude and quantum phase fluctuations. (b) Probability P_g for detecting the atom in level g is recorded, as a function of the Ramsey interferometer phase ϕ, for three different values of the field dephasing angle Φ corresponding to $\delta=712$, 347, and 104 kHz from top to bottom. The average photon number is 9.5. The fringe contrast decreases when the separation of the field components, represented in the insets at right, is increased.

and R_2^{eg} result from the interference of two quantum paths (see Fig. 2). Interference fringes are observed only if nothing in the apparatus allows us to distinguish these two channels. What happens then if C contains a small coherent field nonresonant with the $e\Leftrightarrow g$ transition? Since the phase of this field is kicked by an angle depending upon the atom's state in C, this field acts as a "which path" detector (Scully, Englert, and Walther, 1991; Haroche, 1992) able to reveal the atomic "path" through the Ramsey interferometer. According to the complementarity principle, the fringes then tend to vanish.

This is what we observe (see Fig. 16). When the phase rotation Φ is smaller than the quantum phase fluctuations of the initial field and thus too small to permit one to distinguish the two paths without ambiguity, the fringe contrast is merely reduced. The fringes disappear

altogether when the phase rotation is large, removing all ambiguity regarding the atom's path. The field rotation Φ is adjusted by changing the detuning δ between the atomic transition and the cavity mode. A simple analysis of the experiment shows that the fringe signal is merely multiplied by the scalar product of the two final coherent states $\langle \alpha \exp(-i\Phi) | \alpha \exp(i\Phi) \rangle$. The modulus of this complex number accounts for the fringe contrast reduction, while its phase accounts for the fringe phase shifts apparent in Fig. 16. This phase shift arises from the light shifts experienced by the atom inside the cavity field (Brune *et al.*, 1994). This phase shift provides a direct measurement of the mean photon number $\bar{n} = 9.5$ in this experiment. Note that similar complementarity experiments have been performed in quantum optics with other systems (Eichmann *et al.*, 1993; Pfau *et al.*, 1994; Chapman *et al.*, 1995; Dürr, Nonn, and Rempe, 1998a, 1998b).[5]

C. Decoherence caught in the act

In the previous experiment, we have measured an interference effect characterizing the atomic state superposition, which is influenced by the presence of the field in C. Let us now consider the field state superposition itself. How long does it survive in C? To answer this question, we must analyze in more detail the nature of the field's "environment." Since the field losses are mainly due to photon scattering on mirror surface imperfections, we can describe this environment as being made of the free space around the cavity, which can be filled by the scattered photons. If the cavity contains on average $\bar{n}$ photons, a small field with about one photon escapes in the environment within a characteristic time $T_r / \bar{n}$. This microscopic field is entangled through its phase with the field remaining in C.

This entanglement with the environment provides a way to determine, at least in principle, the phase of the field in C. The phase of the tiny component escaping to the outside world, could, in principle, be measured, reducing the field left in C to one or the other term, thereby destroying the quantum coherence.[6] This is the very essence of the decoherence phenomenon as analyzed by W. Zurek (1991). Thus, after a time of the order of $T_r / \bar{n}$, the quantum coherence between the two field

components in C has vanished. This explains why macroscopic fields, corresponding to huge $\bar{n}$ values, behave classically, since they experience a quasi-instantaneous decoherence process. In our experiment, however, $\bar{n}$ is of the order of 3 to 10 only. The decoherence time is then long enough to allow for the observation of transient interference signals associated with the two components of our Schrödinger cat state in C. Note that these conclusions do not depend on the details of the cavity relaxation. If the field losses occurred by absorption in the mirrors, instead of by photon scattering, the electronic degrees of freedom in the mirrors would get entangled with the field, leading to the same dynamics for the decoherence process.

To observe decoherence in action, we send in C, a delay τ after the first atom A_1 which prepares the "cat state," a second atom A_2, playing so to speak the role of a "quantum mouse" used to probe in C the quantum coherence of the field. This second atom kicks in turn the phase of the field components in C, recombining them partially. This recombination produces, in a correlation signal between the two atoms, an interference term sensitive to the quantum coherence between the cat-state components left by the first atom in C (Brune *et al.*, 1996). The $A_1 - A_2$ correlation signal, $\eta = P(e_2/e_1) - P(e_2/g_1)$, is the difference of the conditional probabilities for finding A_2 in e provided A_1 has been detected either in e or g. The correlation η is independent of the Ramsey phase ϕ under the experimental conditions. It should be ideally 0.5 if the cavity contains a quantum superposition of coherent components and 0 after the decoherence process is completed.

The experimental correlation signal, $\eta(\tau)$, is shown in Fig. 17 as a function of the time delay τ between A_1 and A_2 for two "cat" configurations pictorially depicted in the insets. As expected, the correlation decreases when τ is increased. This phenomenon occurs faster and faster when the two components of the cat are separated more and more. This provides a direct illustration of the main features of environment-induced decoherence, which acts faster and faster as the size of the system becomes more and more macroscopic. Note the good agreement between the experimental points and the theoretical curves, deduced from a very simple calculation based on decoherence theory (Raimond *et al.*, 1997; Maître *et al.*, 1997). This experiment, which verifies the main aspect of the decoherence theory, constitutes a step in the exploration of the quantum/classical boundary. Similar Schrödinger cat experiments (Monroe *et al.*, 1996) and decoherence studies (Myatt *et al.*, 2000) have been performed with an ion in a trap. In this case, however, the loss of coherence was due to the perturbing effect of a classical noise acting on the system and not to quantum entanglement with the environment.

---

[5]Note added. After submission of this review article, we have performed another complementarity experiment in which the coherent field in the cavity itself replaces one of the two Ramsey pulses (Bertet *et al.*, 2001). This field plays then the role of a "quantum beam splitter." When the coherent field contains a small photon number, it is appreciably modified by the emission of one photon by the atom. It then stores information about the atomic "path" in the Ramsey interferometer and no fringes are observed. When the photon number is large, the atom does not sensibly modify the field and fringes are visible.

[6]The fact that this measurement is unrealistic is irrelevant here. The mere fact that the information escapes in an unobserved environment is enough to destroy the quantum coherence of the Schrödinger cat state.
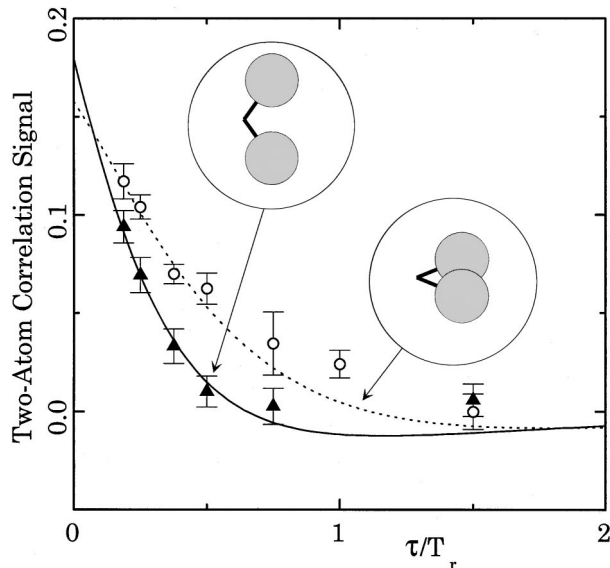
IX. CONCLUSIONS AND PERSPECTIVES

We have described a very flexible and versatile setup to generate and manipulate entanglement on a small ensemble of atoms and photons interacting either via reso-

FIG. 17. Decoherence experiment. Correlation signal η plotted versus the delay, τ, between the two atoms. The initial coherent field contains 3.3 photons on the average. Experimental results for two different values of the field component separation are shown here (circles and triangles). The phase shifts, corresponding to $\delta/2\pi = 170$ and 70 kHz, respectively, are depicted in the insets. The curves result from a simple analytical model.

nant or dispersive interactions. We have prepared EPR pairs (Hagley *et al.*, 1997) of entangled atoms, demonstrated the operation of a quantum gate (Rauschenbeutel *et al.*, 1999) and used it to perform the first quantum nondemolition detection of a single photon (Nogues *et al.*, 1999). Combining up to six operations on four qubits (three atoms and one field mode), we have prepared and studied a GHZ entangled triplet (Rauschenbeutel *et al.*, 2000). In the context of quantum information processing, this experiment constitutes, to our knowledge, the most complex combination so far of successive logic operations involving individually addressable quantum systems. We have also prepared mesoscopic field state superpositions illustrating the main aspects of the Schrödinger cat paradox. By observing directly the evolution of these states, we have confirmed the basic features of environment-induced decoherence theories, in an experiment which provides a glimpse at the quantum/ classical border (Brune *et al.*, 1996).

The present setup, however, suffers experimental limitations: nonideal Ramsey and Rabi pulses limit the fidelity of complex entanglement manipulations. Cavity damping and residual thermal fields contribute also to decoherence processes. Finally, the Poisson statistics of the atomic source leads to prohibitively long data acquisition times for experiments involving more than three particle correlations. Various improvements are under way to overcome these difficulties. Better cavities without ring should allow us to manipulate atomic coherences for longer times and distances. Atomic sources based on cold atom techniques could be used to prepare single atoms on demand (Frese *et al.*, 2000). Finally, the

detection efficiency could be boosted to nearly 100% and the thermal field background completely eliminated.

Among the possible experiments under way or under consideration, let us mention tests of quantum nonlocality with massive particles [EPR, GHZ, and more complex multiparticle situations (Mermin, 1990)], quantum teleportation of atomic quantum states (Davidovich *et al.*, 1994), unrestricted quantum nondemolition of photon numbers via dispersive interactions (Brune *et al.*, 1990), measurement of the Wigner function of nonclassical field states (Lutterbach *et al.*, 1997; Nogues *et al.*, 2000), cavity-assisted collisions between two or more Rydberg atoms, leading to other forms of qubit entanglement (Zheng and Guo, 2000). With deterministic single atom sources, more complex manipulations of entanglement as well as the implementation of simple quantum algorithms or error correction codes will become possible. In these experiments the scalability implied by single particle addressing will be an asset.

Finally, we are also considering in the long term experiments coupling two cavities via their interactions with a single atom. Two mesoscopic fields at macroscopic distances could thus be entangled, a situation which would marry the "strangeness" of the EPR and Schrödinger cat situations.

REFERENCES

Aspect, A., 1999, Nature (London) **398**, 189.

Aspect, A., J. Dalibard, and G. Roger, 1982, Phys. Rev. Lett. **49**, 1804.

Bell, J. S., 1964, Physics (Long Island City, N.Y.) **1**, 195.

Bencheick, K., J. A. Levenson, P. Grangier, and O. Lopez, 1995, Phys. Rev. Lett. **75**, 3422.

Bennett, C. H., G. Brassard, C. Crépeau, R. Jozsa, A. Peres, and W. K. Wootters, 1993, Phys. Rev. Lett. **70**, 1895.

Berman, P., 1994, Ed., *Cavity Quantum Electrodynamics* (Academic Press).

Bertet, P., S. Osnaghi, A. Rauschenbeutel, G. Nogues, A. Auffeves, M. Brune, J. M. Raimond, and S. Haroche, 2001, Nature (London) **411**, 166.

Bertoni, A., P. Bordone, R. Brunetti, C. Jacoboni, and S. Reggiani, 2000, Phys. Rev. Lett. **84**, 5912.

Bohm, D., 1951, *Quantum Theory* (Prentice-Hall, Englewood Cliffs, NJ), pp. 614–623.

Boschi, D., S. Branca, F. De Martini, L. Hardy, and S. Popescu, 1998, Phys. Rev. Lett. **80**, 1121.

Bouchiat, V., D. Vion, P. Joyez, D. Estève, and M. H. Devoret, 1999, J. Supercond. **12**, 789.

Bouwmeester, D., J.-W. Pan, K. Mattle, M. Eibl, H. Weinfurter, and A. Zeilinger, 1998, Nature (London) **390**, 575.

Braginsky, V. B., and F. Y. Khalili, 1992, in *Quantum Measurement*, edited by K. S. Thorne (Cambridge University Press, Cambridge).

Braginsky, V. B., Yu. I. Vorontsov, and F. Y. Khalili, 1977, Zh. Eksp. Teor. Fiz. **78**, 1712 [Sov. Phys. JETP **46**, 705 (1977)].

Braunstein, S. L., C. M. Caves, R. Jozsa, N. Linden, S. Popescu, and R. Schack, 1999, Phys. Rev. Lett. **83**, 1054.

Bruckmeier, R., H. Hansen, and S. Schiller, 1997, Phys. Rev. Lett. **79**, 1463.

Brune, M., E. Hagley, J. Dreyer, X. Maître, A. Maali, C. Wunderlich, J. M. Raimond, and S. Haroche, 1996b, Phys. Rev. Lett. **77**, 4887.

Brune, M., S. Haroche, V. Lefèvre, J. M. Raimond, and N. Zagury, 1990, Phys. Rev. Lett. **65**, 976.

Brune, M., P. Nussenzveig, F. Schmidt-Kaler, F. Bernardot, A. Maali, J. M. Raimond, and S. Haroche, 1994, Phys. Rev. Lett. **72**, 3339.

Brune, M., F. Schmidt-Kaler, A. Maali, J. Dreyer, E. Hagley, J. M. Raimond, and S. Haroche, 1996a, Phys. Rev. Lett. **76**, 1800.

Caldeira, A. O., and A. J. Leggett, 1983, Physica A **121**, 587.

Caves, C. M., K. S. Thorne, R. W. P. Drever, V. D. Sandberg, and M. Zimmermann, 1980, Rev. Mod. Phys. **52**, 341.

Chapman, M. S., T. D. Hammond, A. Lenef, J. Schmiedmayer, R. A. Rubenstein, E. Smith, and D. E. Pritchard, 1995, Phys. Rev. Lett. **75**, 3783.

Davidovich, L., N. Zagury, M. Brune, J. M. Raimond, and S. Haroche, 1994, Phys. Rev. A **50**, R895.

DiVincenzo, D. P., 1995, Science **270**, 255.

Dürr, S., T. Nonn, and G. Rempe, 1998a, Nature (London) **395**, 33.

Dürr, S., T. Nonn, and G. Rempe, 1998b, Phys. Rev. Lett. **81**, 5705.

Eberly, J. H., N. B. Narozhny, and J. J. Sanchez-Mondragon, 1980, Phys. Rev. Lett. **44**, 1323.

Ekert, A., 1991, Phys. Rev. Lett. **67**, 661.

Ekert, A., and R. Josza, 1996, Rev. Mod. Phys. **68**, 733.

Ekert, A., and C. Macchiavelo, 1996, Phys. Rev. Lett. **77**, 2585.

Eichmann, U., J. C. Bergquist, J. J. Bollinger, J. M. Gilligan, W. M. Itano, and D. J. Wineland, 1993, Phys. Rev. Lett. **70**, 2359.

Einstein, A., B. Podolsky, and N. Rosen, 1935, Phys. Rev. **47**, 777.

Frese, D., B. Ueberholz, S. Kuhr, W. Alt, D. Schrader, V. Gomer, and D. Meschede, 2000, Phys. Rev. Lett. **85**, 3777.

Friedman, J. R., V. Patel, W. Chen, S. K. Tolpygo, and J. E. Lukens, 2000, Nature (London) **406**, 43.

Furusawa, A., J. L. Sörensen, S. L. Braunstein, C. A. Fuchs, H. J. Kimble, and E. S. Polzik, 1998, Science **282**, 706.

Gershenfeld, N. A., and I. L. Chuang, 1997, Science **275**, 350.

Glauber, R. J., 1963, Phys. Rev. **131**, 2766.

Grangier, P., A. L. Levenson, and J. P. Poizat, 1998, Nature (London) **396**, 537.

Greenberger, D. M., M. A. Horne, and A. Zeilinger, 1990, Am. J. Phys. **58**, 1131.

Gross, M., and J. Liang, 1986, Phys. Rev. Lett. **57**, 3160.

Grover, L. K., 1997, Phys. Rev. Lett. **79**, 325.

Hagley, E., X. Maître, G. Nogues, C. Wunderlich, M. Brune, J. M. Raimond, and S. Haroche, 1997, Phys. Rev. Lett. **79**, 1.

Haroche, S., 1992, in *Fundamental Systems in Quantum Optics, les Houches summer school session LIII*, edited by J. Dalibard, J. M. Raimond, and J. Zinn-Justin (North-Holland, Amsterdam).

Haroche, S., M. Brune, and J. M. Raimond, 1992, Appl. Phys. B: Photophys. Laser Chem. **54**, 355.

Haroche, S., and J. M. Raimond, 1994, in *Cavity Quantum Electrodynamics*, edited by P. Berman (Academic Press), p. 123.

Haroche, S., and J. M. Raimond, 1996, Phys. Today **49** (8), p. 51.

Hood, C. J., T. W. Lynn, A. C. Doherty, A. S. Parkins, and H. J. Kimble, 2000, Science **287**, 1447.

Hulet, R. G., and D. Kleppner, 1983, Phys. Rev. Lett. **51**, 1430.

Jaynes, E. T., and F. W. Cummings, 1963, Proc. IEEE **51**, 89.

Jennewein, T., C. Simon, G. Wiehs, H. Weinfurter, and A. Zeilinger, 2000, Phys. Rev. Lett. **84**, 4729.

Jones, J. A., M. Mosca, and R. H. Hansen, 1998, Nature (London) **393**, 344.

Kim, J. I., K. M. Fonseca Romero, A. M. Horiguti, L. Davidovich, M. C. Nemes, and A. F. R. de Toledo Piza, 1999, Phys. Rev. Lett. **82**, 4737.

La Porta, A., R. E. Slusher, and B. Yurke, 1989, Phys. Rev. Lett. **62**, 28.

Levenson, M. D., R. M. Shelby, M. Reid, and D. F. Walls, 1986, Phys. Rev. Lett. **57**, 2473.

Lloyd, S., 1996, Science **273**, 1073.

Lutterbach, L. G., and L. Davidovich, 1997, Phys. Rev. Lett. **78**, 2547.

Maître, X., E. Hagley, J. Dreyer, A. Maali, C. Wunderlich, M. Brune, J. M. Raimond, and S. Haroche, 1997, J. Mod. Opt. **44**, 2023.

Maître, X., E. Hagley, G. Nogues, C. Wunderlich, P. Goy, M. Brune, J. M. Raimond, and S. Haroche, 1997, Phys. Rev. Lett. **79**, 769.

Mermin, N. D., 1990, Phys. Rev. Lett. **65**, 1838.

Monroe, C., D. M. Meekhof, B. E. King, W. M. Itano, and D. J. Wineland, 1995, Phys. Rev. Lett. **75**, 4714.

Monroe, C., D. M. Meekhof, B. E. King, and D. J. Wineland, 1996, Science **272**, 1131.

Münstermann, P., T. Fischer, P. Maunz, P. W. H. Pinkse, and G. Rempe, 1999, Phys. Rev. Lett. **82**, 3791.

Myatt, C. J., B. E. King, Q. A. Turchette, C. A. Sackett, D. Kielpinski, W. M. Itano, C. Monroe, and D. J. Wineland, 2000, Nature (London) **403**, 269.

Naik, D. S., C. G. Peterson, A. G. White, A. J. Berglund, and P. G. Kwiat, 2000, Phys. Rev. Lett. **84**, 4733.

Nogues, G., A. Rauschenbeutel, S. Osnaghi, P. Bertet, M. Brune, J. M. Raimond, S. Haroche, L. G. Lutterbach, and L. Davidovich, 2000, Phys. Rev. A **62**, 054101.

Nogues, G., A. Rauschenbeutel, S. Osnaghi, M. Brune, J. M. Raimond, and S. Haroche, 1999, Nature (London) **400**, 239.

Nussenzveig, P., F. Bernardot, M. Brune, J. Hare, J. M. Raimond, S. Haroche, and W. Gawlik, 1993, Phys. Rev. A **48**, 3991.

Omnès, R., 1994, *The Interpretation of Quantum Mechanics* (Princeton University, Princeton, NJ).

Pan, J.-W., D. Bouwmeester, M. Daniell, H. Weinfurter, and A. Zeilinger, 2000, Nature (London) **403**, 515.

Pfau, T., S. Spälter, Ch. Kurtsiefer, C. R. Ekstrom, and J. Mlynek, 1994, Phys. Rev. Lett. **73**, 1223.

Raimond, J. M., 2000, http://www.lkb.ens.fr/recherche/qedcav/english/englishframes.html.

Raimond, J. M., M. Brune, and S. Haroche, 1997, Phys. Rev. Lett. **79**, 1964.

Raimond, J. M., and S. Haroche, 1999, in *International Trends in Optics and Photonics, ICO IV*, edited by T. Asakura (Springer Verlag, Berlin), p. 40.

Raithel, G., C. Wagner, H. Walther, L. M. Narducci, and M. O. Scully, 1994, in *Cavity Quantum Electrodynamics*, edited by P. Berman (Academic, New York), p. 57.

Ramsey, N. F., 1985, *Molecular Beams* (Oxford University Press, New York).

Rarity, J. G., P. C. M. Owens, and P. R. Tapster, 1994, J. Mod. Opt. **41**, 2435.

Rauch, H., A. Zeilinger, G. Badurek, and A. Wilfing, 1975, Phys. Lett. **54A**, 425.

Rauschenbeutel, A., G. Nogues, S. Osnaghi, P. Bertet, M. Brune, J. M. Raimond, and S. Haroche, 1999, Phys. Rev. Lett. **83**, 5166.

Rauschenbeutel, A., G. Nogues, S. Osnaghi, P. Bertet, M. Brune, J. M. Raimond, and S. Haroche, 2000, Science **288**, 2024.

Rempe, G., H. Walther, and N. Klein, 1987, Phys. Rev. Lett. **58**, 353.

Roch, J. F., K. Vigneron, Ph. Grelu, A. Sinatra, J.-Ph. Poizat, and Ph. Grangier, 1997, Phys. Rev. Lett. **78**, 634.

Rowe, M. A., D. Kielpinski, V. Meyer, C. A. Sackett, W. M. Itano, C. Monroe, and D. J. Wineland, 2001, Nature (London) **409**, 791.

Sackett, C. A., D. Kielpinski, B. E. King, C. Langer, V. Meyer, C. J. Myatt, M. Rowe, Q. A. Turchette, W. M. Itano, D. J. Wienland, and C. Monroe, 2000, Nature (London) **404**, 256.

Schack, R., and C. M. Caves, 1999, Phys. Rev. A **60**, 4354.

Schrödinger, E., 1935, Naturwissenschaften **23**, 807.

Scully, M. O., B. E. Englert, and H. Walther, 1991, Nature (London) **351**, 111.

Shor, P. W., 1994, in *Proceedings of the 35th Annual Symposium on the Foundations of Computer Science*, edited by S. Goldwasser (IEEE Computer Society).

Steane, A., 1996, Phys. Rev. Lett. **77**, 793.

Tittle, W., J. Brendel, H. Zbinden, and N. Gisin, 2000, Phys. Rev. Lett. **84**, 4737.

Thompson, R. J., G. Rempe, and H. J. Kimble, 1992, Phys. Rev. Lett. **68**, 1132.

Turchette, Q. A., C. S. Wood, B. E. King, C. J. Myatt, D. Leibfried, W. M. Itano, C. Monroe, and D. J. Wineland, 1998, Phys. Rev. Lett. **81**, 3631.

van der Wal, C. H., A. C. J. ter Haar, F. K. Wilhelm, R. N. Schouten, C. J. P. M. Harmans, T. P. Orlando, S. Lloyd, and J. E. Mooij, 2000, Science **290**, 773.

van Enk, S. J., J. I. Cirac, and P. Zoller, 1997, Phys. Rev. Lett. **78**, 4293.

Varcoe, B., S. Brattke, and H. Walther, 2000, Nature (London) **403**, 743.

Weidinger, M., B. Varcoe, R. Heelein, and H. Walther, 1999, Phys. Rev. Lett. **82**, 3795.

Werner, S. A., R. Colella, A. W. Overhauser, and C. F. Eagen, 1975, Phys. Rev. Lett. **35**, 1053.

Zeilinger, A., 1998, Rev. Mod. Phys. **71**, S288.

Zheng, S. B., and G. C. Guo, 2000, Phys. Rev. Lett. **85**, 2392.

Zurek, W. H., 1981, Phys. Rev. D **24**, 1516.

Zurek, W. H., 1982, Phys. Rev. D **26**, 1862.

Zurek, W. H., 1991, Phys. Today **44** (10), 36.